

# Non-Diagonal and Mixed Squark Production at Hadron Colliders

Giuseppe Bozzi, Benjamin Fuks and Michael Klasen\*

*Laboratoire de Physique Subatomique et de Cosmologie,*

*Université Joseph Fourier/CNRS-IN2P3,*

*53 Avenue des Martyrs, F-38026 Grenoble, France*

(Dated: November 18, 2018)

## Abstract

We calculate squared helicity amplitudes for non-diagonal and mixed squark pair production at hadron colliders, taking into account not only loop-induced QCD diagrams, but also previously unconsidered electroweak channels, which turn out to be dominant. Mixing effects are included for both top and bottom squarks. Numerical results are presented for several SUSY benchmark scenarios at both the CERN LHC and the Fermilab Tevatron, including the possibilities of light stops or sbottoms. The latter should be easily observed at the Tevatron in associated production of stops and sbottoms for a large range of stop masses and almost independently of the stop mixing angle. Asymmetry measurements for light stops at the polarized BNL RHIC collider are also briefly discussed.

arXiv:hep-ph/0507073v1 6 Jul 2005

---

\*klasens@lpsc.in2p3.fr

## I. INTRODUCTION

One of the most promising extensions of the Standard Model (SM) of particle physics is the Minimal Supersymmetric Standard Model (MSSM) [1, 2], which postulates a symmetry between fermionic and bosonic degrees of freedom in nature and predicts the existence of a fermionic (bosonic) supersymmetric (SUSY) partner for each bosonic (fermionic) SM particle. Since SUSY and SM particles contribute to the quadratic divergence of the mass of the Higgs boson with equal strength, but opposite sign, the MSSM can, *inter alia*, stabilize the electroweak energy scale with respect to the Planck scale and thus propose a solution to the hierarchy problem.

Unfortunately, SUSY particles still remain to be discovered. Their masses must therefore be considerably larger than those of the corresponding SM particles, and the symmetry is bound to be broken. In order to remain a viable solution to the hierarchy problem, SUSY can, however, only be broken via soft mass terms in the Lagrangian, with the consequence that the SUSY particle masses should lie in the TeV range and thus within the discovery reach of current and future hadron colliders such as the Tevatron and the LHC.

Due to their strong coupling, squarks should be abundantly produced at hadron colliders. In addition, phase space favors the production of the lighter of the two squark mass eigenstates of identical flavor, which are superpositions of the left- and right-handed helicity eigenstates. Since the off-diagonal elements of the two-dimensional squark mixing matrix are proportional to the mass of the corresponding SM quark, squark mixing is particularly important for third generation squarks. As a consequence, hadroproduction of light stop [3] and, more recently, also light sbottom pairs [4] has received particular theoretical and experimental attention. Mixing effects have also been analyzed recently for slepton, and in particular stau, hadroproduction [5].

As has been observed previously, Quantum Chromodynamics (QCD) alone does not allow for non-diagonal (light plus heavy) squark hadroproduction at tree-level, *i.e.*  $\mathcal{O}(\alpha_s^2)$  in the strong coupling constant  $\alpha_s$ . Non-diagonal squark production rather requires the presence of at least one squark-mixing vertex, such as the four-squark interaction, present, *e.g.*, in final-state rescattering of gluon-induced diagonal squark production. The corresponding finite one-loop diagrams at  $\mathcal{O}(\alpha_s^4)$  have been evaluated in a decoupled gluino scenario with top squark loops only and found to be suppressed with respect to diagonal light/heavy stop

pair production at the Tevatron/LHC by three to six orders of magnitude [3].

In this Paper, we investigate the importance of electroweak channels for non-diagonal and mixed squark pair production at hadron colliders. Naively, one expects these cross sections, which are of  $\mathcal{O}(\alpha^2)$  in the fine structure constant  $\alpha$ , to be smaller than the diagonal strong channels by about two orders of magnitude. For non-diagonal squark production, the interplay between loop suppression in QCD and coupling suppression in the electroweak case merits a detailed investigation. In the presence of the mixing of bottom squarks, their loop contributions must also be taken into account. Mixed top and bottom squark production is possible at tree-level only through an  $s$ -channel exchange of a charged  $W^\pm$ -boson. Observation of this channel may allow for interesting conclusions on the supersymmetric version of the CKM matrix.

Our analytical calculations are presented in Sec. II, where we put in the additional effort to calculate squared amplitudes for definite initial parton helicities to exhibit clearly the mixing angle dependence in the left- and right-handed components of the electroweak currents and to allow for future applications to polarized hadron collisions. To be complete, we present our results for diagonal, non-diagonal, and mixed top and bottom squark hadroproduction with quark and gluon initial states up to  $\mathcal{O}(\alpha_s^4)$  and  $\mathcal{O}(\alpha^2)$ , respectively.

In Sec. III, we choose several typical SUSY mass spectra arising from different SUSY breaking scenarios, including those allowing for light stops and sbottoms, and apply them to the Tevatron and the LHC. Cross sections are presented as functions of the squark masses, mixing angles, and general SUSY breaking mass parameters. We also briefly discuss possible asymmetry measurements for light stops at the polarized RHIC collider. Our conclusions are given in Sec. IV, and squark mixing is discussed in App. A.

It is not the aim of this work to present a full signal-to-background analysis of non-diagonal and mixed squark production, as this is best done within the experimental collaborations and using full detector simulations. Rather, our analytical results lend themselves easily to implementation in general purpose Monte Carlo programs such as PYTHIA [6] or HERWIG [7], which are traditionally employed for these kinds of simulations.

## II. ANALYTICAL RESULTS

In the following, we present the leading contributions in the strong ( $\alpha_s$ ) and electromagnetic ( $\alpha$ ) coupling constant to the color-averaged cross sections  $d\hat{\sigma}_{h_a, h_b}$  for definite helicities  $h_a$  and  $h_b$  of the initial partons  $a$  and  $b$ . We define the square of the weak coupling constant  $g_W^2 = e^2/\sin^2\theta_W$  in terms of the electromagnetic fine structure constant  $\alpha = e^2/(4\pi)$  and the squared sine of the electroweak mixing angle  $x_W = \sin^2\theta_W$ . The coupling strengths of left- and right-handed (s)quarks to the neutral electroweak current are then given by

$$L_q = 2T_q^3 - 2e_q x_W \quad \text{and} \quad R_q = -2e_q x_W, \quad (1)$$

where the weak isospin quantum numbers are  $T_q^3 = \pm 1/2$  for left-handed and  $T_q^3 = 0$  for right-handed up- and down-type (s)quarks, and their fractional electromagnetic charges are denoted by  $e_q$ .

In general SUSY breaking models, where the squark interaction eigenstates are not identical to the respective mass eigenstates, the coupling strengths  $L_q$  and  $R_q$  must be multiplied by  $S_{j1}S_{i1}^*$  and  $S_{j2}S_{i2}^*$ , respectively, where  $i, j \in \{1, 2\}$  label the squark mass eigenstates (conventionally  $m_{\tilde{q}_1} < m_{\tilde{q}_2}$ ) and  $S$  represents the unitary matrix diagonalizing the squark mass matrix (see App. A). In the following, the dependence on the squark mixing angle  $\theta_{\tilde{q}}$  will, however, be presented explicitly.

Our results for the strong or electroweak  $2 \rightarrow 2$  scattering processes

$$a_{h_a}(p_a)b_{h_b}(p_b) \rightarrow \tilde{q}_i(p_1)\tilde{q}_j^{(\prime)*}(p_2) \quad (2)$$

with  $a, b = q, \bar{q}, g$  will be expressed in terms of the squark masses  $m_{\tilde{q}_{i,j}^{(\prime)}}$ , the conventional Mandelstam variables,

$$s = (p_a + p_b)^2 \quad , \quad t = (p_a - p_1)^2 \quad , \quad \text{and} \quad u = (p_a - p_2)^2, \quad (3)$$

and the masses of the neutral and charged electroweak gauge bosons  $m_Z$  and  $m_W$ . Unpolarized cross sections, averaged over initial spins, can then easily be derived from the expression

$$d\hat{\sigma} = \frac{d\hat{\sigma}_{1,1} + d\hat{\sigma}_{1,-1} + d\hat{\sigma}_{-1,1} + d\hat{\sigma}_{-1,-1}}{4}, \quad (4)$$

while single and double polarized cross sections, including the same average factor for initial spins, are given by

$$d\Delta\hat{\sigma}_L = \frac{d\hat{\sigma}_{1,1} + d\hat{\sigma}_{1,-1} - d\hat{\sigma}_{-1,1} - d\hat{\sigma}_{-1,-1}}{4} \quad (5)$$

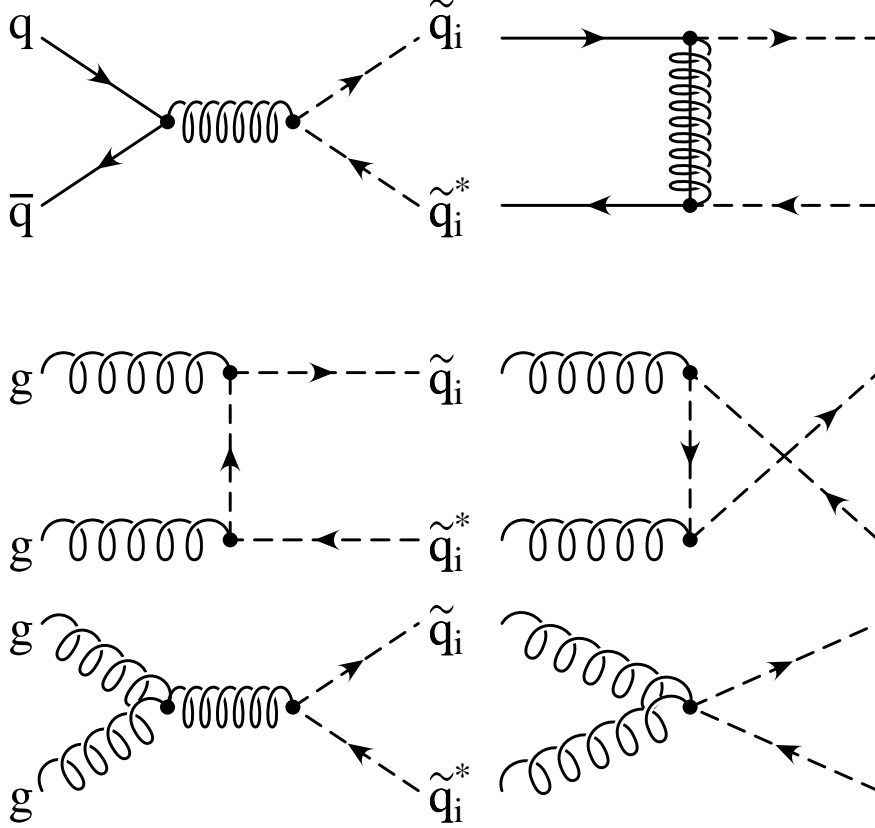


FIG. 1: Tree-level QCD Feynman diagrams for diagonal squark production at hadron colliders. The upper right diagram is absent for top squarks due to the negligible top quark density in the proton.

and

$$d\Delta\hat{\sigma}_{LL} = \frac{d\hat{\sigma}_{1,1} - d\hat{\sigma}_{1,-1} - d\hat{\sigma}_{-1,1} + d\hat{\sigma}_{-1,-1}}{4}, \quad (6)$$

so that the the single and double longitudinal spin asymmetries become

$$A_L = \frac{d\Delta\hat{\sigma}_L}{d\hat{\sigma}} \quad \text{and} \quad A_{LL} = \frac{d\Delta\hat{\sigma}_{LL}}{d\hat{\sigma}}. \quad (7)$$

### A. Diagonal top and bottom squark production

For diagonal top and bottom squark production, we consider only the dominant tree-level strong coupling channels shown in Fig. 1. For next-to-leading order QCD corrections to diagonal top squark production see Ref. [3]. Other exchanges are significantly suppressed by smaller electroweak or Yukawa couplings. For the two upper diagrams, initiated by

quarks, we find

$$\begin{aligned}
\frac{d\hat{\sigma}_{h_a, h_b}^{q\bar{q}}}{dt} &= \frac{4\pi\alpha_s^2}{9s^2} [1 - h_a h_b] \frac{tu - m_{\tilde{q}}^4}{s^2} \\
&- \frac{4\pi\alpha_s^2}{27s^2} [1 \pm (h_b - h_a) \cos 2\theta_{\tilde{q}} - h_a h_b] \frac{tu - m_{\tilde{q}}^4}{st_{\tilde{g}}} \delta_{qb} \delta_{\tilde{q}\tilde{b}} \\
&+ \frac{\pi\alpha_s^2}{18s^2} \left[ \frac{(1 + h_a h_b)(1 - \cos 4\theta_{\tilde{q}}) m_{\tilde{g}}^2 s + (1 - h_a h_b)(3 + \cos 4\theta_{\tilde{q}})(tu - m_{\tilde{q}}^4)}{t_{\tilde{g}}^2} \right. \\
&\quad \left. \pm 4 \cos 2\theta_{\tilde{q}} (h_b - h_a) \frac{tu - m_{\tilde{q}}^4}{t_{\tilde{g}}^2} \right] \delta_{qb} \delta_{\tilde{q}\tilde{b}}, \tag{8}
\end{aligned}$$

where the upper sign holds for  $\tilde{b}_1$  and the lower sign for  $\tilde{b}_2$  production. Stops are produced only through  $s$ -channel gluon exchange due to negligible top quark parton density functions (PDFs) in the proton. Even for sbottom production,  $t$ -channel gluino contributions are suppressed by small bottom PDFs and the heavy gluino propagator,  $t_{\tilde{g}}^{-1} = (t - m_{\tilde{g}}^2)^{-1}$ , where  $m_{\tilde{g}}$  is the gluino mass. In the case of no squark mixing, our results agree with the double-polarized and unpolarized cross sections in Ref. [8].

For the four lower diagrams in Fig. 1, initiated by gluons, we find

$$\frac{d\hat{\sigma}_{h_a, h_b}^{gg}}{dt} = \frac{\pi\alpha_s^2}{128s^2} \left[ 24 \left( 1 - 2 \frac{t_{\tilde{q}} u_{\tilde{q}}}{s^2} \right) - \frac{8}{3} \right] \left[ (1 - h_a h_b) - 2 \frac{sm_{\tilde{q}}^2}{t_{\tilde{q}} u_{\tilde{q}}} \left( (1 - h_a h_b) - \frac{sm_{\tilde{q}}^2}{t_{\tilde{q}} u_{\tilde{q}}} \right) \right], \tag{9}$$

where  $t_{\tilde{q}} = t - m_{\tilde{q}}^2$  and  $u_{\tilde{q}} = u - m_{\tilde{q}}^2$ , independently of the squark mixing angle and thus in direct agreement with the double-polarized and unpolarized cross sections of Ref. [8].

## B. Non-diagonal top and bottom squark production

Due to the non-chiral strong interaction of the gluon, non-diagonal squark pairs cannot be produced in QCD at tree-level with either  $q\bar{q}$  or  $gg$  initial states. There are, however, quark-induced chiral tree-level electroweak and supersymmetric interactions, proceeding either through an  $s$ -channel  $Z$ -boson exchange (see Fig. 2) or a  $t$ -channel gluino or neutralino exchange (see Fig. 3). As in the case of diagonal squark production,  $t$ -channel exchanges are present only for bottom squarks, due to negligible top quark PDFs, and even there they are suppressed by small bottom PDFs and the heavy gluino or neutralino propagators, where the latter are defined by  $t_{\tilde{\chi}_k^0}^{-1} = (t - m_{\tilde{\chi}_k^0}^2)^{-1}$ .  $m_{\tilde{\chi}_k^0}$  is the mass of the  $k^{\text{th}}$  neutralino mass eigenstate, which couples with strength

$$\{L_{\tilde{q}i}, R_{\tilde{q}i}^*\} = \pm \left[ e_q \sqrt{x_W(1 - x_W)} N'_{i1} + (T_{qL,R}^3 - e_q x_W) N'_{i2} \right] \tag{10}$$

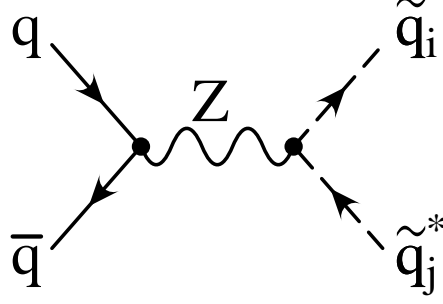


FIG. 2: Dominant tree-level electroweak Feynman diagram for non-diagonal ( $i \neq j$ ) squark production at hadron colliders.

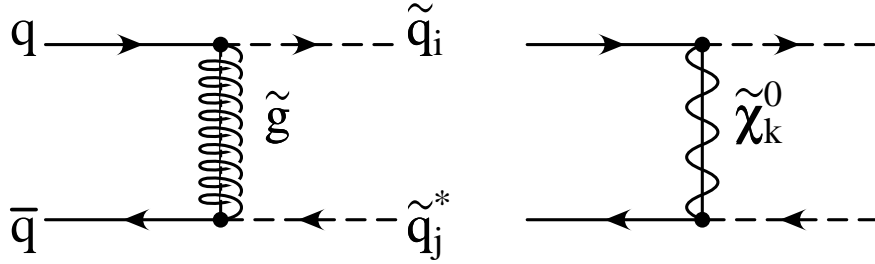


FIG. 3: Feynman diagrams for non-diagonal ( $i \neq j$ ) squark production at hadron colliders proceeding through  $t$ -channel gluino (left) and neutralino (right) exchange.

to left- and right-handed (s)quarks, if we neglect the relatively small bottom Yukawa couplings. The unitary matrix  $N'$  diagonalizes the neutralino mass matrix in the photino-zino basis [9]. Gluino exchanges are, in contrast, enhanced by the strong coupling constant  $\alpha_s$ .

Our analytical result up to  $\mathcal{O}(\alpha^2)$  and  $\mathcal{O}(\alpha_s^2)$  for  $s$ - and  $t$ -channel exchanges, including interferences, is

$$\begin{aligned}
\frac{d\hat{\sigma}_{h_a, h_b}^{q\bar{q}}}{dt} = & \frac{\pi\alpha^2}{s^2} \left[ \frac{tu - m_{\tilde{q}_1}^2 m_{\tilde{q}_2}^2}{s^2} \right] \frac{\sin^2(2\theta_{\tilde{q}}) \left[ (1-h_a)(1+h_b)L_q^2 + (1+h_a)(1-h_b)R_q^2 \right]}{32x_W^2(1-x_W)^2(1-m_Z^2/s)^2} \\
& - \frac{\pi\alpha\alpha_s}{s^2} \left[ \frac{tu - m_{\tilde{q}_1}^2 m_{\tilde{q}_2}^2}{st_{\tilde{g}}} \right] \frac{\sin^2(2\theta_{\tilde{q}}) \left[ (1-h_a)(1+h_b)L_q - (1+h_a)(1-h_b)R_q \right]}{9x_W(1-x_W)(1-m_Z^2/s)} \delta_{qb} \delta_{\tilde{q}\tilde{b}} \\
& + \frac{\pi\alpha_s^2}{9s^2} \left[ \frac{[(1+h_a h_b)(3 + \cos 4\theta_{\tilde{q}}) - 4(h_a + h_b) \cos 2\theta_{\tilde{q}}] m_{\tilde{g}}^2 s}{t_{\tilde{g}}^2} \right. \\
& \quad \left. + \frac{2 \sin^2 2\theta_{\tilde{q}} (1 - h_a h_b) (tu - m_{\tilde{q}_1}^2 m_{\tilde{q}_2}^2)}{t_{\tilde{g}}^2} \right] \delta_{qb} \delta_{\tilde{q}\tilde{b}} \\
& - \frac{\pi\alpha^2}{s^2} \sum_i \delta_{qb} \delta_{\tilde{q}\tilde{b}} \left[ \frac{tu - m_{\tilde{q}_1}^2 m_{\tilde{q}_2}^2}{st_{\tilde{\chi}_i^0}} \right] \frac{\sin^2(2\theta_{\tilde{q}}) \left[ (1-h_a)(1+h_b)L_q L_{\tilde{q}_i}^2 - (1+h_a)(1-h_b)R_q R_{\tilde{q}_i}^2 \right]}{12x_W^2(1-x_W)^2(1-m_Z^2/s)}
\end{aligned}$$

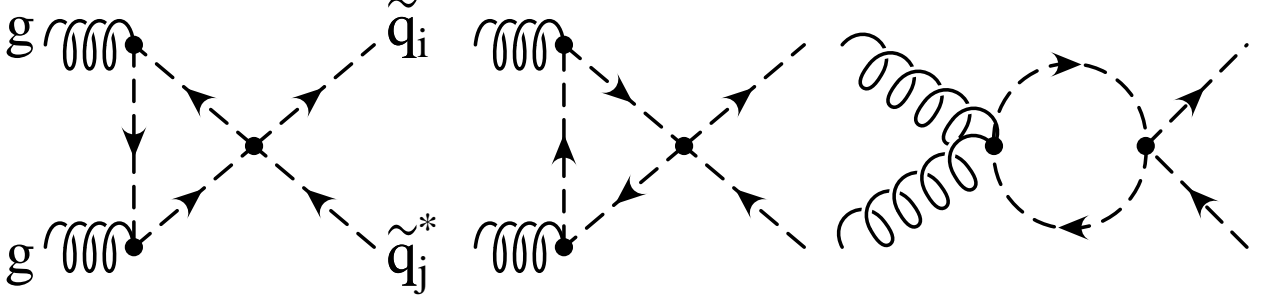


FIG. 4: Subdominant loop-level QCD Feynman diagrams for non-diagonal ( $i \neq j$ ) squark production at hadron colliders.

$$\begin{aligned}
& + \frac{\pi\alpha^2}{s^2} \sum_{i,j} \frac{\delta_{qb} \delta_{\tilde{q}\tilde{b}}}{1 + \delta_{ij}} \left[ \frac{[(1 + h_a h_b)(3 + \cos 4\theta_{\tilde{q}}) - 4(h_a + h_b) \cos 2\theta_{\tilde{q}}] L_{\tilde{q}i} L_{\tilde{q}j} R_{\tilde{q}i} R_{\tilde{q}j} m_{\tilde{\chi}_i^0} m_{\tilde{\chi}_j^0} s}{x_W^2 (1 - x_W)^2 t_{\tilde{\chi}_i^0} t_{\tilde{\chi}_j^0}} \right. \\
& \left. + \frac{\sin^2 2\theta_{\tilde{q}} [(1 - h_a)(1 + h_b) L_{\tilde{q}i}^2 L_{\tilde{q}j}^2 + (1 + h_a)(1 - h_b) R_{\tilde{q}i}^2 R_{\tilde{q}j}^2] (tu - m_{\tilde{q}_1}^2 m_{\tilde{q}_2}^2)}{x_W^2 (1 - x_W)^2 t_{\tilde{\chi}_i^0} t_{\tilde{\chi}_j^0}} \right], \quad (11)
\end{aligned}$$

where we have summed over  $\tilde{q}_1 \tilde{q}_2^* + \tilde{q}_2 \tilde{q}_1^*$  final states. Note that there is no neutralino-gluino interference term due to color (non-)conservation.

Within QCD and in the limit of a decoupled gluino, the only possibility to produce non-diagonal squark pairs is by rescattering of diagonal squark pairs through four-squark vertices in the final state. The corresponding Feynman diagrams, shown in Fig. 4, have (one-)loop topology and are therefore suppressed by additional squark propagators and/or annihilations within the squark loop. The squared helicity amplitude for the production of non-diagonal stop pairs in gluon-gluon collisions is given by

$$\begin{aligned}
\frac{d\hat{\sigma}_{h_a, h_b}^{gg}}{dt} &= (1 + h_a h_b) \left[ \frac{37\alpha_s^4 \sin^2(4\theta_{\tilde{t}})}{27648\pi s^4} |\Delta \ln_{\tilde{t}}|^2 \right. \\
&+ \sum_{\tilde{q} \neq \tilde{t}} \frac{5\alpha_s^4 \cos^2(2\theta_{\tilde{q}}) \sin^2(2\theta_{\tilde{t}})}{3072\pi s^4} |\Delta \ln_{\tilde{q}}|^2 \\
&+ \sum_{\tilde{q} \neq \tilde{t}} \frac{5\alpha_s^4 \cos(2\theta_{\tilde{q}}) \cos(2\theta_{\tilde{t}}) \sin^2(2\theta_{\tilde{t}})}{2304\pi s^4} \text{Re}(\Delta \ln_{\tilde{q}} \Delta \ln_{\tilde{t}}) \\
&+ \left. \sum_{\tilde{q}, \tilde{q}' \neq \tilde{t}; \tilde{q} \neq \tilde{q}'} \frac{5\alpha_s^4 \cos(2\theta_{\tilde{q}}) \cos(2\theta_{\tilde{q}'} \sin^2(2\theta_{\tilde{t}})}{1536\pi s^4} \text{Re}(\Delta \ln_{\tilde{q}} \Delta \ln_{\tilde{q}'} \right), \quad (12)
\end{aligned}$$

where  $\Delta \ln_{\tilde{q}} = m_{\tilde{q}_1}^2 \ln^2(-x_{\tilde{q}_1}) - m_{\tilde{q}_2}^2 \ln^2(-x_{\tilde{q}_2})$ ,

$$x_{\tilde{q}_i} = \frac{1 - \beta_{\tilde{q}_i}}{1 + \beta_{\tilde{q}_i}}, \quad (13)$$



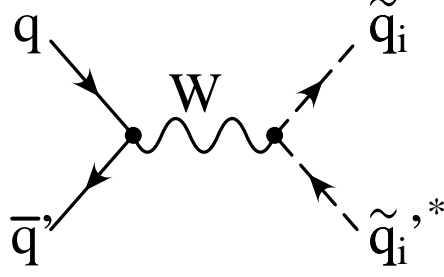


FIG. 5: Dominant electroweak Feynman diagram for mixed (*e.g.* top and bottom) squark production at hadron colliders.

and  $\beta_{\tilde{q}_i} = \sqrt{1 - 4m_{\tilde{q}_i}^2}$  is the velocity of the  $i^{\text{th}}$  squark mass eigenstate. In the limit of degenerate light squarks, only top and bottom squark loops survive loop annihilations, and the squared helicity amplitude simplifies to

$$\begin{aligned} \frac{d\hat{\sigma}_{h_a, h_b}^{gg}}{dt} = & (1 + h_a h_b) \left[ \frac{37\alpha_s^4 \sin^2(4\theta_{\tilde{t}})}{27648\pi s^4} |\Delta \ln_{\tilde{t}}|^2 \right. \\ & + \frac{5\alpha_s^4 \cos^2(2\theta_{\tilde{b}}) \sin^2(2\theta_{\tilde{t}})}{3072\pi s^4} |\Delta \ln_{\tilde{b}}|^2 \\ & \left. + \frac{5\alpha_s^4 \cos(2\theta_{\tilde{b}}) \cos(2\theta_{\tilde{t}}) \sin^2(2\theta_{\tilde{t}})}{2304\pi s^4} \text{Re}(\Delta \ln_{\tilde{b}} \Delta \ln_{\tilde{t}}) \right]. \end{aligned} \quad (14)$$

These expressions have been summed over  $\tilde{t}_1 \tilde{t}_2^* + \tilde{t}_2 \tilde{t}_1^*$  final states and generalize the corresponding result in Ref. [3], where only top squark loops were taken into account. For non-diagonal sbottom production, top and bottom squark indices have to be exchanged in the equations above.

### C. Mixed top and bottom squark production

As mentioned above, mixed top and bottom squark production proceeds at tree-level only through an  $s$ -channel exchange of a charged  $W^\pm$ -boson, shown in Fig. 5. The exchange of a  $t$ -channel chargino is excluded by negligible top quark PDFs in the proton, and  $t$ -channel gluino contributions are loop-suppressed, since they require electroweak rescattering of the intermediate squarks. The squared helicity amplitude is therefore

$$\frac{d\hat{\sigma}_{h_a, h_b}^{q\bar{q}'}}{dt} = \frac{\pi\alpha^2}{s^2} |V_{qq'}|^2 |V_{\tilde{t}_1 \tilde{b}_1}|^2 \left[ \frac{tu - m_{\tilde{t}_1}^2 m_{\tilde{b}_1}^2}{s^2} \right] \frac{\cos^2 \theta_{\tilde{t}} \cos^2 \theta_{\tilde{b}} (1 - h_a)(1 + h_b)}{4x_W^2 (1 - m_W^2/s)^2}, \quad (15)$$

where we show explicitly the dependence on the SM and SUSY CKM matrix elements. Here, we have *not* summed over  $\tilde{t}_1 \tilde{b}_1^* + \tilde{b}_1 \tilde{t}_1^*$  final states, since each of them is produced by different

partonic luminosities of the correct weak isospin partners  $q$  and  $\bar{q}'$  in initial state. This purely left-handed charged current cross section is easily derived from the squared  $s$ -channel contribution in Eq. (11) by adjusting the squark masses, including the squared absolute values of the appropriate CKM matrix elements  $V_{qq'}$  and  $V_{\tilde{t}_1\tilde{b}_1}$  and by setting

$$m_Z \rightarrow m_W, \quad R_q = 0, \quad L_q = \sqrt{2} \cos^2 \theta_W, \quad \text{and} \quad \sin^2(2\theta_{\tilde{q}}) \rightarrow 4 \cos^2 \theta_{\tilde{t}} \cos^2 \theta_{\tilde{b}}. \quad (16)$$

For the mixed production of the heavier squark mass eigenstates, the corresponding index 1 has to be replaced by 2 and the squared cosine of the mixing angle by the squared sine. At lowest order, gluon initial states do not allow for the production of a (charged) mixed squark final state.

### III. NUMERICAL RESULTS

We now turn to our numerical results for the production of diagonal, non-diagonal, and mixed squark pairs at hadron colliders and use the squared helicity amplitudes given in Sec. II together with Eq. (4) to calculate unpolarized partonic cross sections. The QCD factorization theorem then allows to compute unpolarized hadronic cross sections

$$\sigma = \int_{m^2/S}^1 d\tau \int_{-1/2 \ln \tau}^{1/2 \ln \tau} dy \int_{t_{\min}}^{t_{\max}} dt f_{a/A}(x_a, M_a^2) f_{b/B}(x_b, M_b^2) \frac{d\hat{\sigma}}{dt} \quad (17)$$

by convolving the relevant partonic cross section  $d\hat{\sigma}$  with universal parton densities  $f_{a/A}$  and  $f_{b/B}$  of partons  $a, b$  in the hadrons  $A, B$ . The PDFs depend on the longitudinal momentum fractions of the two partons  $x_{a,b} = \sqrt{\tau} e^{\pm y}$  and on the unphysical factorization scales  $M_{a,b}$ . We use the most recent leading order (LO) PDF set by the CTEQ collaboration, CTEQ6L1 [10], at the factorization scale  $M_a = M_b = m = (m_{\tilde{q}_i} + m_{\tilde{q}_j^{(\prime)}})/2$  and identify the latter with the renormalization scale  $\mu$  in the strong coupling constant  $\alpha_s(\mu)$ . The QCD scale parameter  $\Lambda$  in the CTEQ6L1 fit for  $n_f = 5$  active quark flavors is 165 MeV.

For the masses and widths of the electroweak gauge bosons, we use the current values of  $m_Z = 91.1876$  GeV,  $m_W = 80.425$  GeV,  $\Gamma_Z = 2.4952$  GeV, and  $\Gamma_W = 2.124$  GeV. The squared sine of the electroweak mixing angle

$$\sin^2 \theta_W = 1 - m_W^2/m_Z^2 \quad (18)$$

and the electromagnetic fine structure constant

$$\alpha = \sqrt{2} G_F m_W^2 \sin^2 \theta_W / \pi \quad (19)$$

can then be calculated in the improved Born approximation using the world average value of  $G_F = 1.16637 \cdot 10^{-5} \text{ GeV}^{-2}$  for Fermi's coupling constant [11]. For the SM CKM matrix elements, we take the central values in Ref. [11], while we set the (so far unknown) SUSY CKM matrix elements  $V_{\tilde{t}_i \tilde{b}_j}$  to one.

The physical masses of the produced squark mass eigenstates and mixing angles are calculated using the recently updated computer program SUSPECT [12]. Its Version 2.3 includes now a consistent calculation of the Higgs mass, with all one-loop and the dominant two-loop radiative corrections, in the renormalization group equations, that link the restricted set of SUSY breaking parameters at the gauge coupling unification scale to the complete set of observable SUSY masses and mixing angles at the electroweak scale. We choose two recently proposed minimal supergravity (mSUGRA) points, SPS 1a and SPS 5, as benchmarks for our numerical study [13].

SPS 1a is a typical mSUGRA point with an intermediate value of  $\tan \beta = 10$  and  $\mu > 0$ . It has a model line attached to it, which is specified by  $m_0 = -A_0 = 0.4 m_{1/2}$ . We vary the common fermion mass  $m_{1/2}$  from 100 GeV, where  $m_{\tilde{t}_1} = 177 \text{ GeV}$  and  $m_{\tilde{b}_1} = 229 \text{ GeV}$  lie already considerably above the current exclusion limits of 95.7 and 89 GeV [11], to 300 GeV for the Tevatron (Fig. 6) and 500 GeV for the LHC (Fig. 7), respectively. At the benchmark point,  $m_{1/2} = 250 \text{ GeV}$ , leading to relatively heavy  $\tilde{t}_1$  and  $\tilde{b}_1$  masses of 399 and 521 GeV.

With the limited Tevatron center-of-mass energy of  $\sqrt{S} = 1.96 \text{ TeV}$ , non-diagonal and mixed squark production will be difficult to discover. As one can see in Fig. 6, only diagonal production of the lighter top squark mass eigenstate will be visible in the full region of the mSUGRA parameter space shown here with the expected final integrated luminosity of  $8.9 \text{ fb}^{-1}$ . For diagonal sbottom production, the accessible parameter space is already reduced to  $m_{1/2} \leq 225 \text{ GeV}$ . Non-diagonal and mixed squark production could only be discovered, if the common fermion mass  $m_{1/2}$  is not much larger than 100 GeV. As expected for a  $p\bar{p}$  collider, the cross sections are very much dominated by  $q\bar{q}$  annihilation, even for the diagonal channels, and  $gg$  initial states contribute at most 15% in the case of diagonal light stop production.

The LHC with its much larger center-of-mass energy of  $\sqrt{S} = 14 \text{ TeV}$  and design luminosity of  $300 \text{ fb}^{-1}$  will, in contrast, have no problem in producing all combinations of squarks in sufficient numbers. The hierarchy between the strong diagonal production channels of

$$p \bar{p} \rightarrow \tilde{q}_i \tilde{q}'_j^*, \text{ Tevatron, } \sqrt{S} = 1.96 \text{ TeV}$$

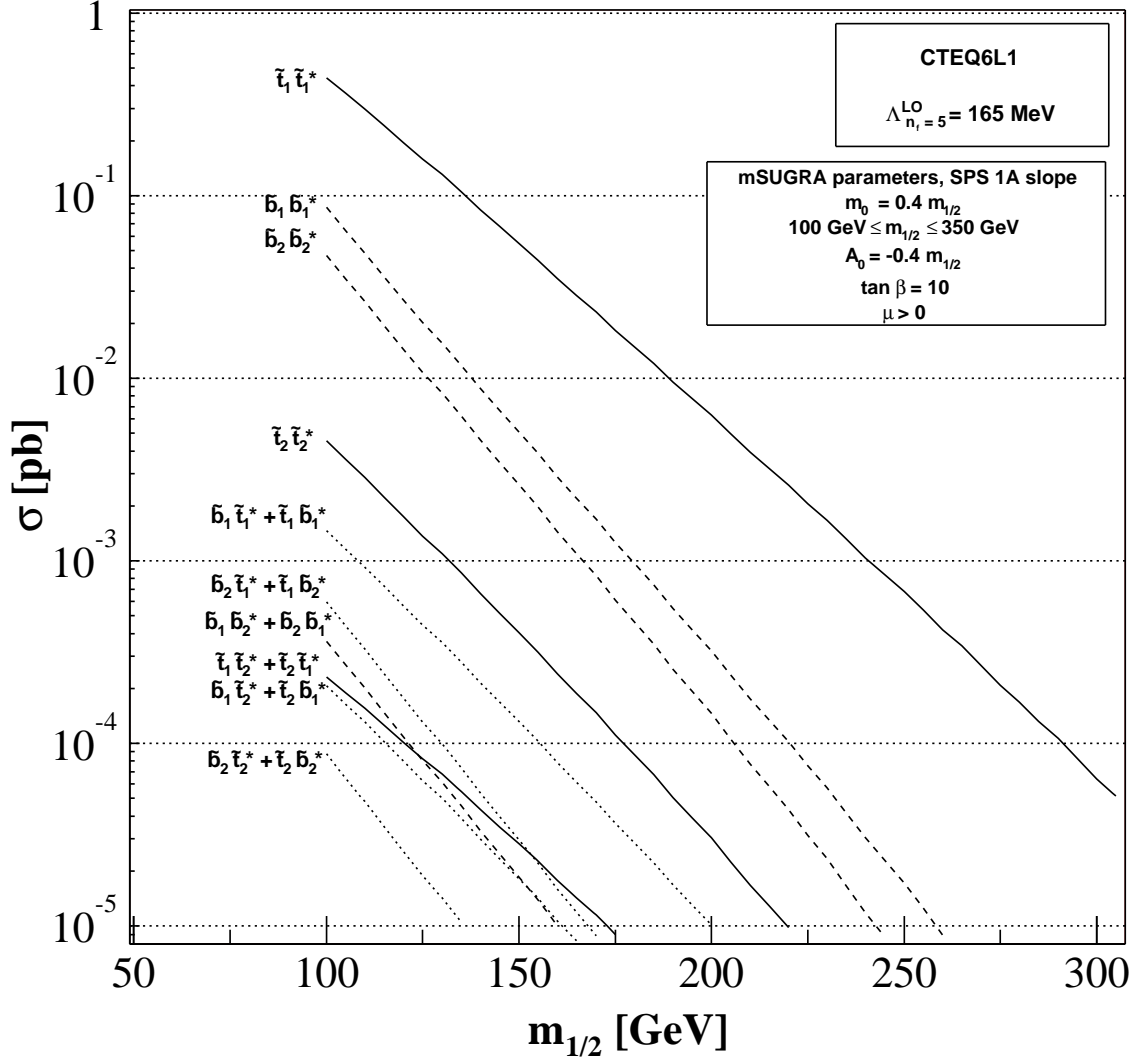


FIG. 6: Production cross sections for top (full), bottom (dashed), and mixed top and bottom squarks (dotted) at the Tevatron as a function of the common fermion mass  $m_{1/2}$  in the mSUGRA model line SPS 1a [13].

$\mathcal{O}(\alpha_s^2)$  and the electroweak non-diagonal and mixed channels of  $\mathcal{O}(\alpha^2)$  is, however, clearly visible in Fig. 7, the latter being about two orders of magnitude smaller. The LHC being a  $pp$  collider and the average  $x$ -value in the PDFs being considerably smaller, the diagonal channels are enhanced by the high  $gg$  luminosity, which dominates their cross sections by up to 93 %. Among the electroweak  $\mathcal{O}(\alpha^2)$  processes, mixed production of top and bottom squarks is favored over non-diagonal top or bottom squark production by the possibility of

$$pp \rightarrow \tilde{q}_i \tilde{q}_j^*, \text{ LHC}, \sqrt{s} = 14 \text{ TeV}$$

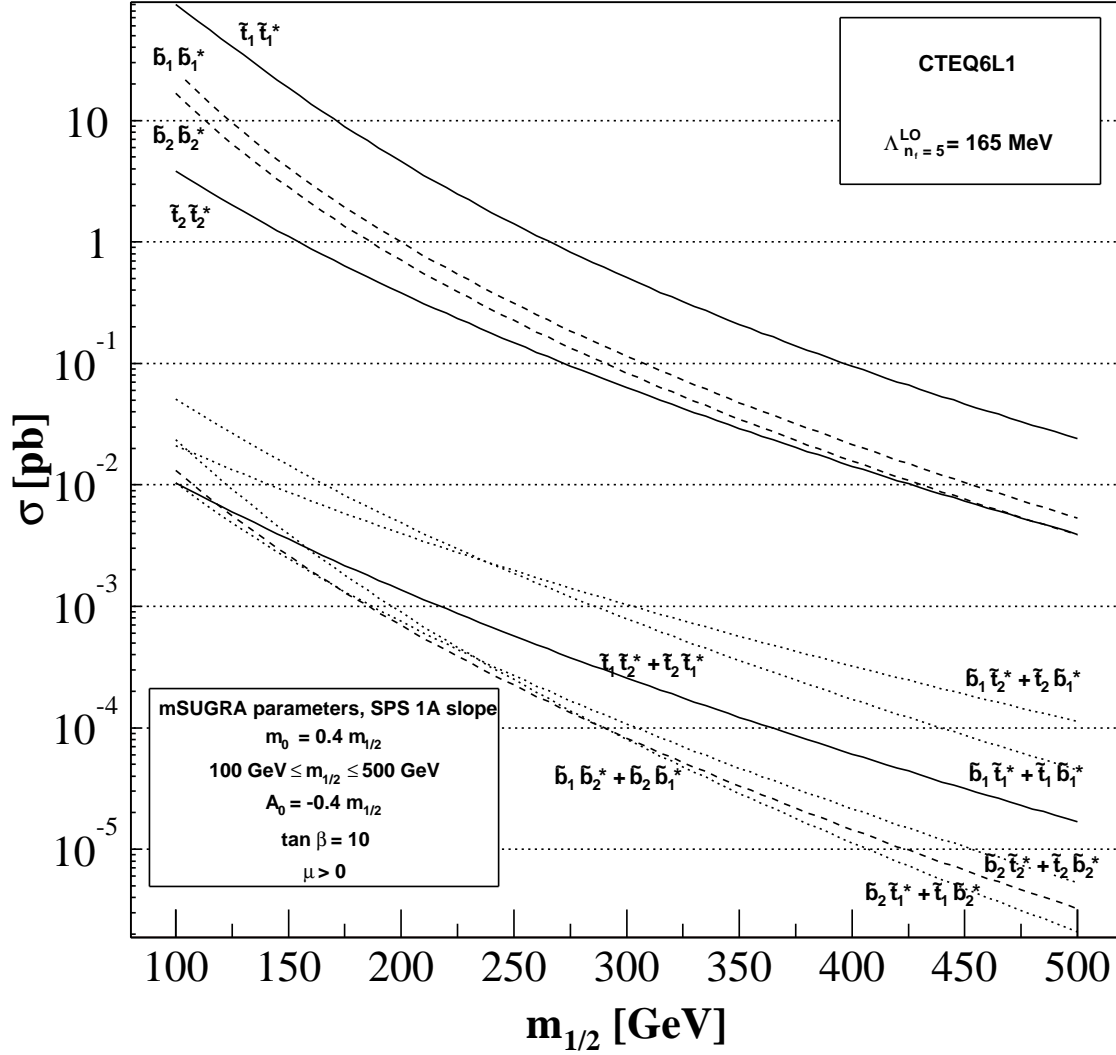


FIG. 7: Production cross sections for top (full), bottom (dashed), and mixed top and bottom squarks (dotted) at the LHC as a function of the common fermion mass  $m_{1/2}$  in the mSUGRA model line SPS 1a [13].

two light masses and a positive charge in the final state, which is more easily produced by the charged  $pp$  initial state.

SPS 5 is a slightly different mSUGRA scenario with lower  $\tan\beta = 5$ , larger  $m_{1/2} = 350$  GeV, and large negative  $A_0 = -1000$  GeV, leading to heavier sbottoms of 566 and 655 GeV, a heavy  $\tilde{t}_2$  of 651 GeV, but also a light  $\tilde{t}_1$  of 259 GeV. Since non-diagonal and mixed squark production will be inaccessible in this case at the Tevatron, we show in Figs. 8 and 9

$$p p \rightarrow \tilde{q}_i \tilde{q}'_j^*, \text{ LHC}, \sqrt{S} = 14 \text{ TeV}$$

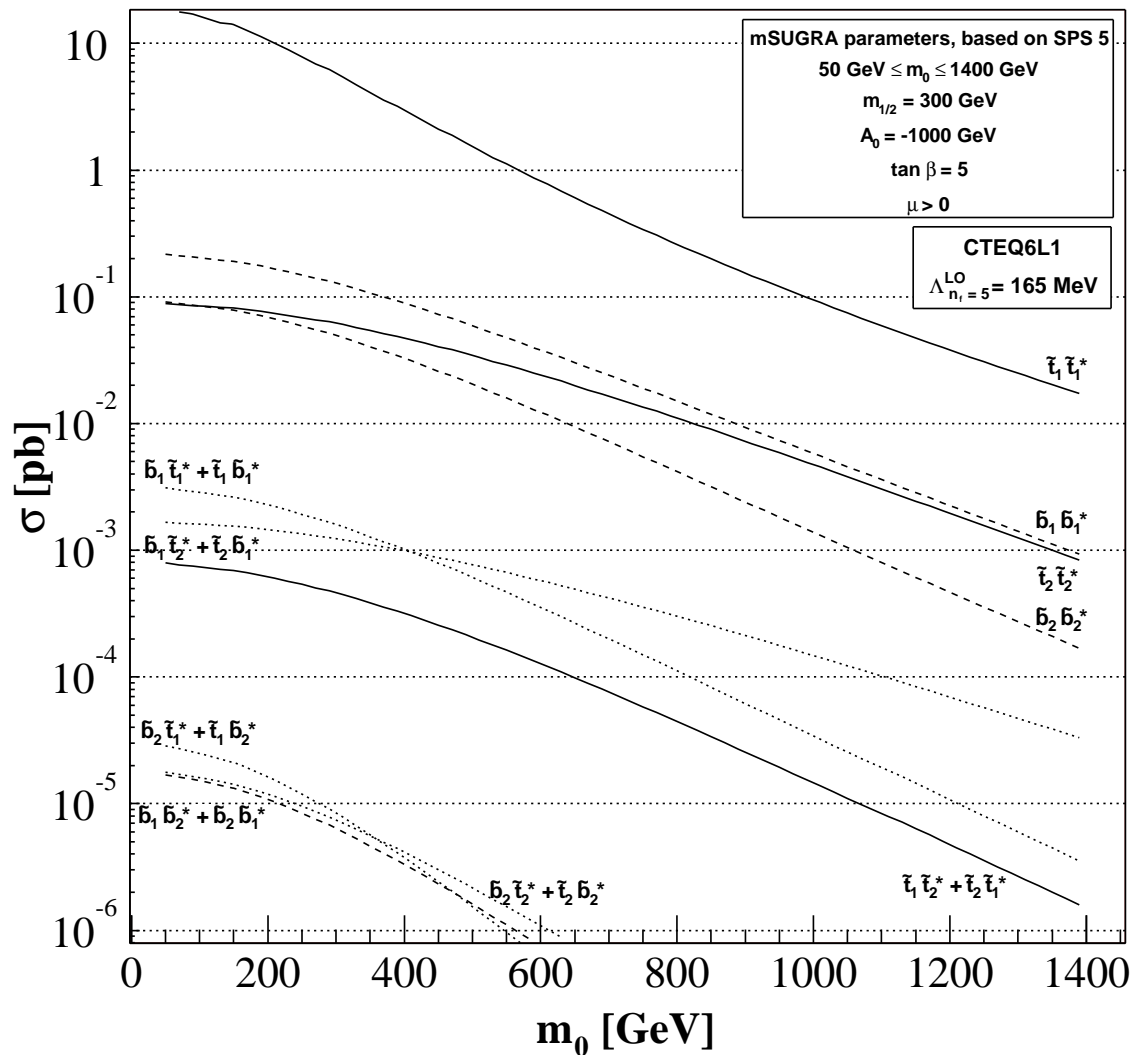


FIG. 8: Production cross sections for top (full), bottom (dashed), and mixed top and bottom squarks (dotted) at the LHC as a function of the scalar mass  $m_0$  in the mSUGRA model SPS 5 [13] with a light top squark.

numerical results for the LHC only, varying either  $m_0$  (Fig. 8) or  $A_0$  (Fig. 9) independently to test the sensitivity of the cross section on the squark masses and mixing.

Concentrating first on the  $m_0$ -dependence, we see in Fig. 8 a clear hierarchy between the dominant pair production of the lighter stop, strong pair production of the heavier stop and sbottoms, charged and neutral electroweak production of final states involving at least one light squark, and finally charged and neutral electroweak production of the heavier squarks,

which may only be visible up to  $m_0 \leq 600$  GeV. The more pronounced hierarchy in Fig. 8 can be explained by the considerable squark mass differences in SPS 5, which lead to additional phase space suppression for the heavier squarks.

As mentioned in the Introduction, the case of non-diagonal squark production merits a more detailed investigation of the relative importance of the coupling-suppressed electroweak diagram in Fig. 2 and the loop-suppressed QCD diagrams in Fig. 4. As mentioned in Sec. II, the  $t$ -channel gluino and neutralino exchange diagrams in Fig. 3 are only present for sbottom production. For the mSUGRA scenario considered here, their contributions are found to be six to eight orders of magnitude smaller than the  $s$ -channel contribution in Fig. 2. While one naively expects the  $\mathcal{O}(\alpha^2)$  and  $\mathcal{O}(\alpha_s^4)$  diagrams in Figs. 2 and 4 to contribute with roughly equal strength, Fig. 9 shows for the case of non-diagonal stop production in the SPS 5 scenario and at the LHC that the QCD loop-contributions are smaller than the electroweak tree-level contribution by about one order of magnitude. This is easily explained by the presence of additional heavy squark propagators in the loop diagrams. Here, we consider not only loops involving top, but also bottom squarks, which do not cancel in Eq. (14), if the masses of the two sbottom mass eigenstates are unequal. However, the non-diagonal elements in the squark mass matrices are proportional to the relevant SM quark mass and  $m_b \ll m_t$ , so that mixing effects are less important for sbottoms than for stops. Consequently, sbottom loops contribute about one order of magnitude less than stop loops, as can also be seen in Fig. 9. SUSY-QCD loop diagrams involving gluino exchanges have not been calculated here, as they are of  $\mathcal{O}(\alpha_s^4)$  and require in addition the presence of heavy top quark and gluino propagators in the loop. In the SPS 5 scenario, we have indeed a heavy gluino of mass  $m_{\tilde{g}} = 725$  GeV. The tree-level cross section in Eq. (11) and the sbottom loop contribution in Eq. (14) depend on the cosine of the stop mixing angle through  $\sin^2(2\theta_{\tilde{t}}) = 4 \cos^2 \theta_{\tilde{t}} (1 - \cos^2 \theta_{\tilde{t}})$ , which is clearly visible in Fig. 9. In contrast, the stop loop contribution in Eq. (14) has a steeper dependence through  $\sin^2(4\theta_{\tilde{t}}) = 16 \cos^2 \theta_{\tilde{t}} (1 - \cos^2 \theta_{\tilde{t}}) (1 - 2 \cos^2 \theta_{\tilde{t}})^2$ , which is also visible in Fig. 9.

The apparent excess of the experimentally observed bottom cross section at the Tevatron over the QCD prediction has led to speculations of light sbottom contributions to this cross section [4], although the use of up-to-date information on the  $B$  fragmentation function may reduce the discrepancy to an acceptable level [14]. Taking the light sbottom scenario at face-value with a sbottom mixing angle of  $\sin \theta_{\tilde{t}} = 0.38$  that reduces its coupling to the  $Z$ -,

$$p p \rightarrow \tilde{t}_1 \tilde{t}_2^* + \tilde{t}_2 \tilde{t}_1^*, \text{ LHC}, \sqrt{S} = 14 \text{ TeV}$$

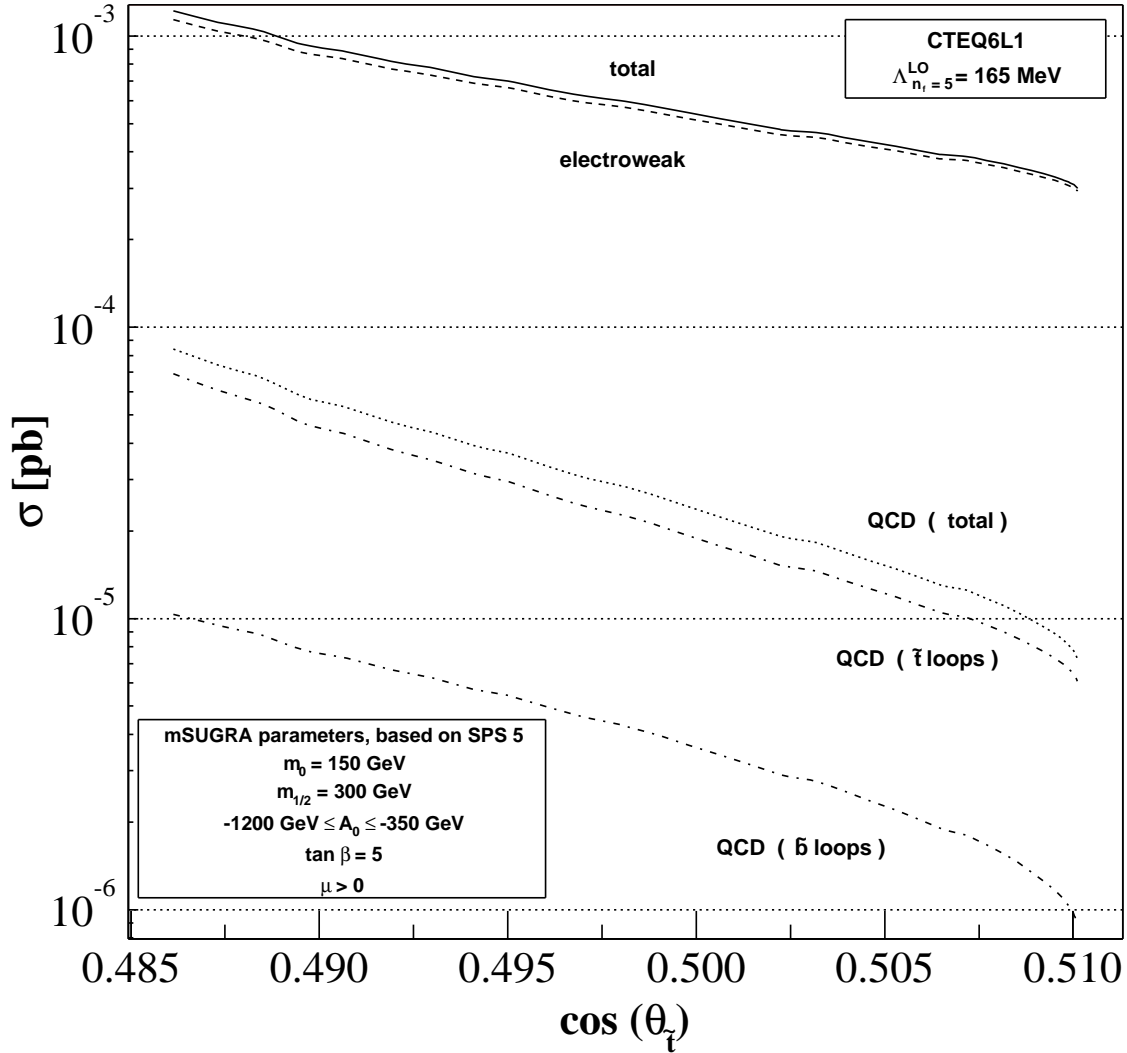


FIG. 9: Contributions of tree-level electroweak and loop-level QCD processes to non-diagonal stop production at the LHC in the mSUGRA model SPS 5 [13] with a light top squark as a function of the cosine of the top squark mixing angle, together with their sums.

but not the  $W$ -boson, we show in Fig. 10 that mixed production of light top and bottom squark mass eigenstates at the Tevatron is yet another promising channel to confirm or exclude this scenario, as the cross section is well visible over a large range of  $\tilde{b}_1$  masses, almost independently of the stop mixing angle and for light ( $m_{\tilde{t}_1} = 100 \text{ GeV}$ ) as well as for heavier ( $m_{\tilde{t}_1} = 400 \text{ GeV}$ ) top squarks.

As a possible application of the polarization dependence of our analytical results, we show



$$p \bar{p} \rightarrow \tilde{t}_1 \tilde{b}_1^* + \tilde{b}_1 \tilde{t}_1^*, \text{ Tevatron, } \sqrt{S} = 1.96 \text{ TeV}$$

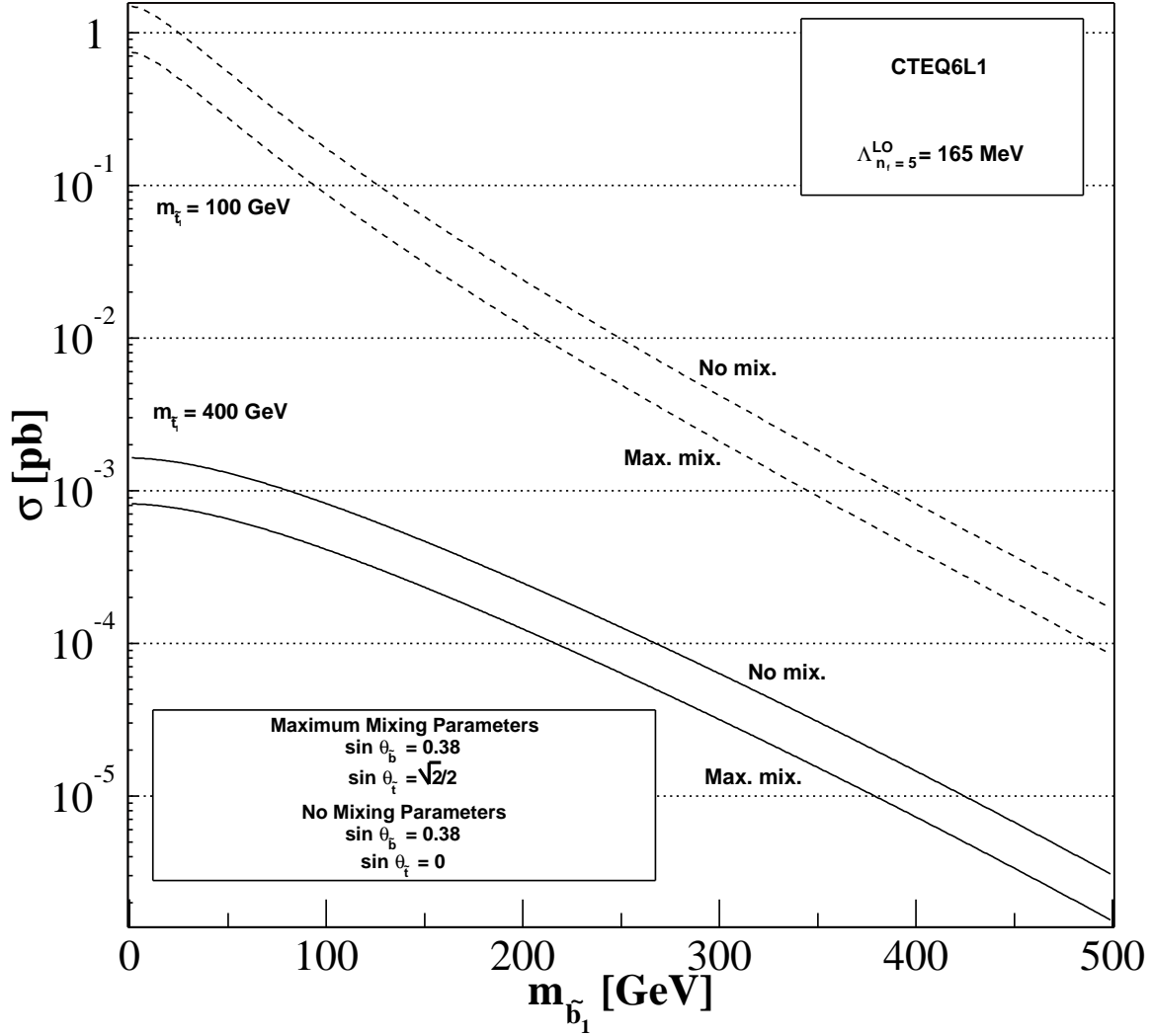


FIG. 10: Associated production of top and bottom squarks at the Tevatron as a function of a light sbottom mass [4] for  $m_{\tilde{t}_1} = 100$  GeV (dashed) and 400 GeV (full) and no (top) or maximal (bottom) top squark mixing.

finally in Fig. 11 the double-spin asymmetry of diagonal light stop production at RHIC. As this polarized  $pp$  collider has only a rather small center-of-mass energy of  $\sqrt{S} = 500$  GeV, the observable stop mass range is obviously very limited. Already for  $m_{\tilde{t}_1} > 106$  GeV, the unpolarized cross section drops below 1 fb, while stop masses below 96 GeV are most likely already excluded [11]. This leaves only a very small mass window of 10 GeV for possible observations. In Fig. 11 one can clearly see the rise of the asymmetry for  $q\bar{q}$  and  $gg$  initial

$$p p \rightarrow \tilde{t}_1 \tilde{t}_1^*, \text{RHIC}, \sqrt{S} = 500 \text{ GeV}$$

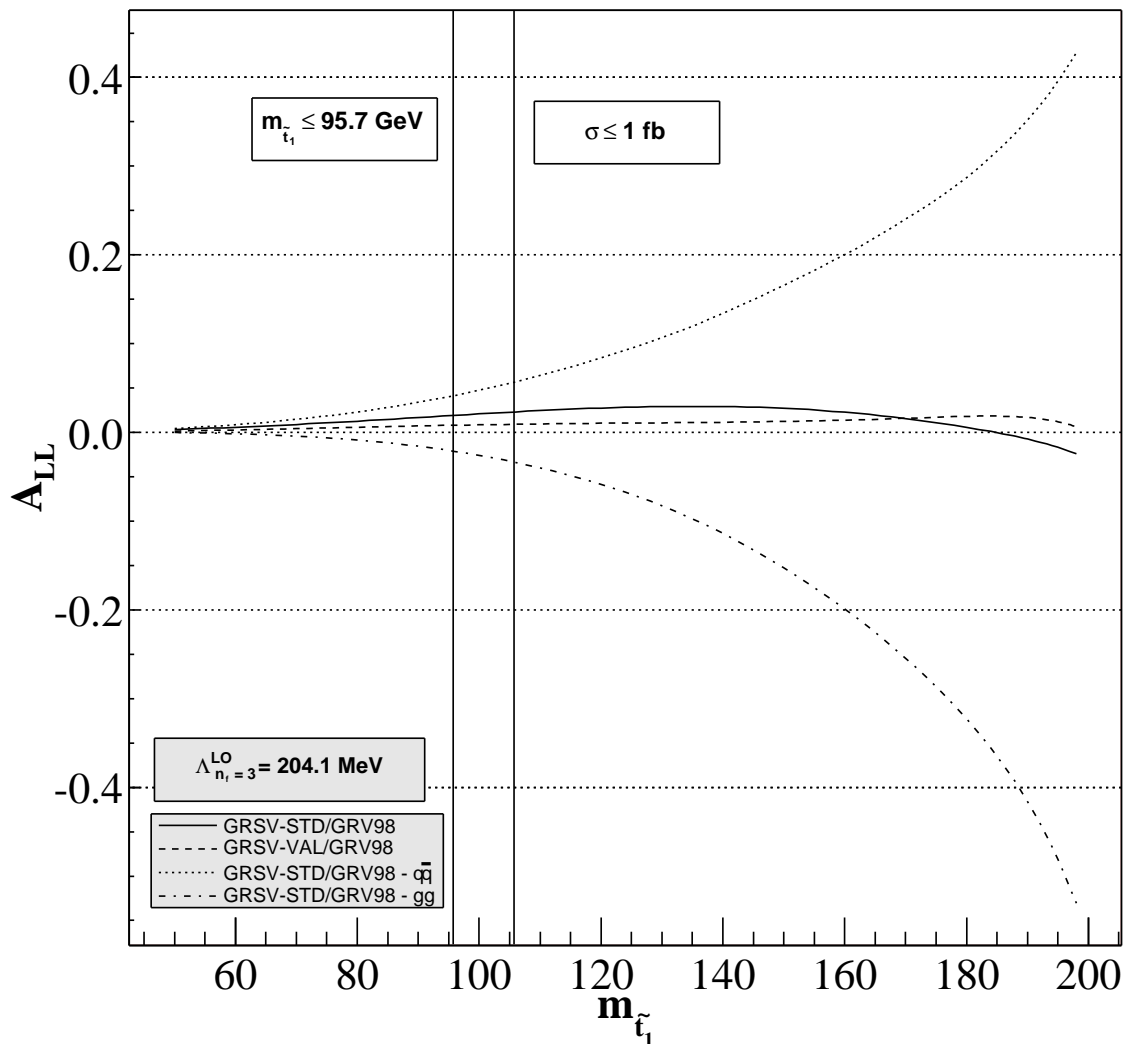


FIG. 11: Contributions of the  $q\bar{q}$  (dotted) and  $gg$  (dot-dashed) initial states to the longitudinal double-spin asymmetry  $A_{LL}$  at RHIC, together with their sum (full), for stop pair production as a function of the light top squark mass. The total asymmetry using GRSV-VAL (dashed) instead of GRSV-STD (full) parton densities [15] is also shown.

states, as the stop mass and the correlated  $x$ -value in the PDFs grows. However, as the two asymmetries are approximately of equal size, but opposite sign, the total observable asymmetry rests below the 5% level in the entire mass range shown. This is true for both choices of polarized parton densities, GRSV 2000 standard (STD) as well as valence (VAL) [15]. For consistency, the unpolarized cross sections have been calculated in this case using

the GRV 98 parton density set [16].

#### IV. CONCLUSION

In Summary, we have presented in this Paper the most extensive analysis to date of diagonal, non-diagonal, and mixed squark production at hadron colliders. Great care has been taken to include in all cases the dominant contributions mediated not only by strong, but also by electroweak interactions up to  $\mathcal{O}(\alpha_s^4)$  and  $\mathcal{O}(\alpha^2)$ , respectively. Squared helicity amplitudes have been presented for all considered channels in analytic form, as they expose the left- and right-handed contributions in the electroweak channels, allow for future applications to polarized hadron collisions, and may easily be implemented in general purpose Monte Carlo programs.

Numerically, we have focused on top and bottom squark production, including mixing in both cases, at the Tevatron and the LHC. We have emphasized the fact that associated light sbottom and stop production may allow for confirmation or exclusion of light sbottom scenarios at the Tevatron. In more traditional scenarios such as the SPS 1a or SPS 5 models, non-diagonal and mixed squark production can probably only be studied at the LHC, where these channels may allow for additional constraints on SUSY masses, mixing angles, or the SUSY CKM matrix.

*Note added in proof:* After presentation of our work at the GDR SUSY conference in Grenoble [17] and at the Cortona 2005 Theoretical Physics Meeting [18], and while this Paper was being completed, a second publication related to the mixed top and bottom squark production aspects of our paper appeared [19]. Unfortunately, the authors do not present any cross section formulæ, so that analytical comparisons are impossible. However, we have checked that our calculations agree with their numerical  $s$ -channel results in Tab. I. Note that real emission contributions such as those labeled  $t$ -channel in Tab. I, coming from gluon initial states, cannot be reliably calculated separately, as they partially contain initial-state singularities that must be absorbed in the proton PDFs, so that these contributions must be included in a complete next-to-leading order calculation.

## Acknowledgments

We thank S. Calvet and T. Millet for valuable discussions at the GDR SUSY conference in Grenoble. This work was supported by a postdoctoral and a Ph.D. fellowship of the French ministry for education and research.

## APPENDIX A: SQUARK MIXING

The (generally complex) soft SUSY-breaking terms  $A_q$  of the trilinear Higgs-squark-squark interaction and the (also generally complex) off-diagonal Higgs mass parameter  $\mu$  in the MSSM Lagrangian induce mixing of the left- and right-handed squark eigenstates  $\tilde{q}_{L,R}$  of the electroweak interaction into mass eigenstates  $\tilde{q}_{1,2}$ . The squark mass matrix [2, 9]

$$\mathcal{M}^2 = \begin{pmatrix} m_{LL}^2 + m_q^2 & m_q m_{LR}^* \\ m_q m_{LR} & m_{RR}^2 + m_q^2 \end{pmatrix} \quad (\text{A1})$$

with

$$m_{LL}^2 = (T_q^3 - e_q \sin^2 \theta_W) m_Z^2 \cos 2\beta + m_{\tilde{Q}}^2, \quad (\text{A2})$$

$$m_{RR}^2 = e_q \sin^2 \theta_W m_Z^2 \cos 2\beta + \begin{cases} m_{\tilde{U}}^2 & \text{for up - type squarks,} \\ m_{\tilde{D}}^2 & \text{for down - type squarks,} \end{cases} \quad (\text{A3})$$

$$m_{LR} = A_q - \mu^* \begin{cases} \cot \beta & \text{for up - type squarks} \\ \tan \beta & \text{for down - type squarks} \end{cases} \quad (\text{A4})$$

is diagonalized by a unitary matrix  $S$ ,  $S\mathcal{M}^2 S^\dagger = \text{diag}(m_1^2, m_2^2)$ , and has the squared mass eigenvalues

$$m_{1,2}^2 = m_q^2 + \frac{1}{2} \left( m_{LL}^2 + m_{RR}^2 \mp \sqrt{(m_{LL}^2 - m_{RR}^2)^2 + 4m_q^2 |m_{LR}|^2} \right). \quad (\text{A5})$$

For real values of  $m_{LR}$ , the squark mixing angle  $\theta_{\tilde{q}}$ ,  $0 \leq \theta_{\tilde{q}} \leq \pi/2$ , in

$$S = \begin{pmatrix} \cos \theta_{\tilde{q}} & \sin \theta_{\tilde{q}} \\ -\sin \theta_{\tilde{q}} & \cos \theta_{\tilde{q}} \end{pmatrix} \quad \text{with} \quad \begin{pmatrix} \tilde{q}_1 \\ \tilde{q}_2 \end{pmatrix} = S \begin{pmatrix} \tilde{q}_L \\ \tilde{q}_R \end{pmatrix} \quad (\text{A6})$$

can be obtained from

$$\tan 2\theta_{\tilde{q}} = \frac{2m_q m_{LR}}{m_{LL}^2 - m_{RR}^2}. \quad (\text{A7})$$

If  $m_{LR}$  is complex, one may first choose a suitable phase rotation  $\tilde{q}'_R = e^{i\phi}\tilde{q}_R$  to make the mass matrix real and then diagonalize it for  $\tilde{q}_L$  and  $\tilde{q}'_R$ .  $\tan\beta = v_u/v_d$  is the (real) ratio of the vacuum expectation values of the two Higgs fields, which couple to the up- and down-type (s)quarks. The weak isospin quantum numbers for left-handed up- and down-type (s)quarks with hypercharge  $Y_q = 1/3$  are  $T_q^3 = \{+1/2, -1/2\}$ , whereas  $Y_q = \{4/3, -2/3\}$  and  $T_q^3 = 0$  for right-handed (s)quarks, and their fractional electromagnetic charges are  $e_q = T_q^3 + Y_q/2$ . The soft SUSY-breaking mass terms for left- and right-handed squarks are  $m_{\tilde{Q}}$  and  $m_{\tilde{U}}, m_{\tilde{D}}$ , respectively, and  $m_Z$  is the mass of the neutral electroweak gauge boson  $Z^0$ .

- 
- [1] H. P. Nilles, Phys. Rept. **110** (1984) 1.
  - [2] H. E. Haber and G. L. Kane, Phys. Rept. **117**, 75 (1985).
  - [3] W. Beenakker, M. Krämer, T. Plehn, M. Spira and P. M. Zerwas, Nucl. Phys. B **515**, 3 (1998).
  - [4] E. L. Berger, B. W. Harris, D. E. Kaplan, Z. Sullivan, T. M. P. Tait and C. E. M. Wagner, Phys. Rev. Lett. **86**, 4231 (2001).
  - [5] G. Bozzi, B. Fuks and M. Klasen, Phys. Lett. B **609**, 339 (2005).
  - [6] T. Sjöstrand, L. Lönnblad, S. Mrenna and P. Skands, hep-ph/0308153.
  - [7] G. Corcella *et al.*, hep-ph/0210213.
  - [8] T. Gehrmann, D. Maître and D. Wyler, Nucl. Phys. B **703**, 147 (2004).
  - [9] J. F. Gunion and H. E. Haber, Nucl. Phys. B **272**, 1 (1986) [Erratum-ibid. B **402**, 567 (1993)].
  - [10] J. Pumplin, D. R. Stump, J. Huston, H. L. Lai, P. Nadolsky and W. K. Tung, JHEP **0207**, 012 (2002).
  - [11] S. Eidelman *et al.* [Particle Data Group Collaboration], Phys. Lett. B **592** (2004) 1.
  - [12] A. Djouadi, J. L. Kneur and G. Moultaka, hep-ph/0211331.
  - [13] B. C. Allanach *et al.*, in *Proc. of the APS/DPF/DPB Summer Study on the Future of Particle Physics (Snowmass 2001)* ed. N. Graf, Eur. Phys. J. C **25**, 113 (2002).
  - [14] M. Cacciari and P. Nason, Phys. Rev. Lett. **89**, 122003 (2002).
  - [15] M. Glück, E. Reya, M. Stratmann and W. Vogelsang, Phys. Rev. D **63**, 094005 (2001).
  - [16] M. Glück, E. Reya and A. Vogt, Eur. Phys. J. C **5**, 461 (1998).
  - [17] B. Fuks, *Non-diagonal stop production at hadron colliders*, talk presented at the GDR SUSY conference, Grenoble, France, April 2005.

- [18] G. Bozzi, *Non-diagonal and mixed squark production at hadron colliders*, poster presented at the Cortona 2005 Theoretical Physics Meeting, Cortona, Italy, May 2005.
- [19] D. Berdine and D. Rainwater, hep-ph/0506261.